Title

Improved chemical and mechanical stability of peptoid nanosheets by photo-crosslinking the hydrophobic core

Journal

Chemical Communications, 52(26)

ISSN

1359-7345

Authors

Flood, Dillon

Proulx, Caroline

Robertson, Ellen J

et al.

Publication Date

2016-04-04

DOI

10.1039/c6cc00588h

Peer reviewed

Volume 52 | Number 26 | 4 April 2016 | Pages 4729–4842

ChemComm

Chemical Communications

www.rsc.org/chemcomm

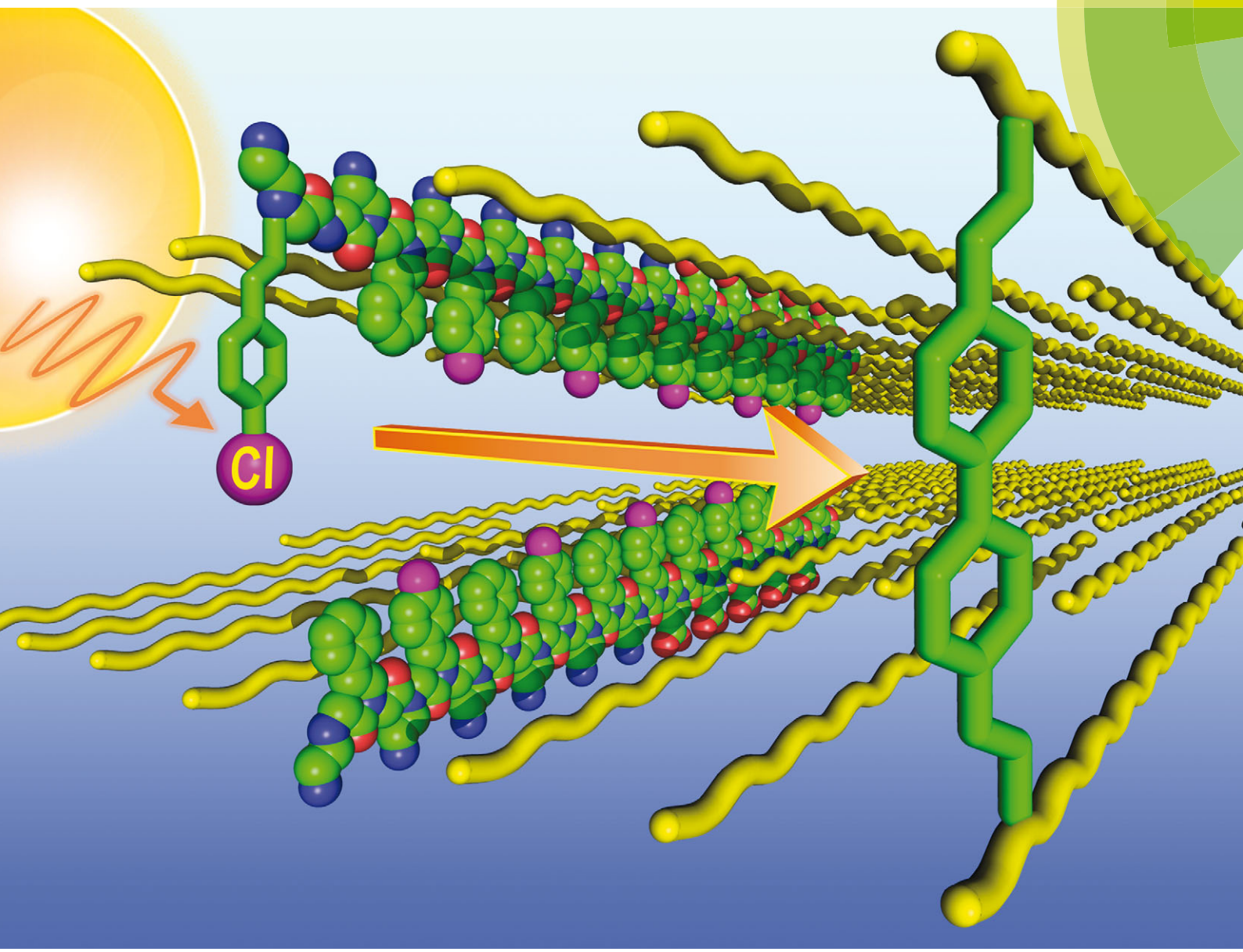

ISSN 1359-7345

ROYAL SOCIETY OF CHEMISTRY

COMMUNICATION

Ronald N. Zuckermann *et al.*

Improved chemical and mechanical stability of peptoid nanosheets by photo-crosslinking the hydrophobic core

175 YEARS

ChemComm

COMMUNICATION

View Article Online
View Journal | View Issue

Cite this: *Chem. Commun.*, 2016, **52**, 4753

Received 21st January 2016,
Accepted 5th February 2016

DOI: 10.1039/c6cc00588h

www.rsc.org/chemcomm

Improved chemical and mechanical stability of peptoid nanosheets by photo-crosslinking the hydrophobic core†

Dillon Flood, Caroline Proulx, Ellen J. Robertson, Alessia Battigelli, Shuo Wang, Adam M. Schwartzberg and Ronald N. Zuckermann*

Peptoid nanosheets can be broadly functionalized for a variety of applications. However, they are susceptible to degradation when exposed to chemical or mechanical stress. To improve their strength, photolabile monomers were introduced in order to crosslink the nanosheet interior. Photo-crosslinking produced a more robust material that can survive sonication, lyophilization, and other biochemical manipulations.

The ability to engineer robust biologically relevant nanomaterials with atomically defined structures is a major step towards the creation of synthetic biomolecules that mimic the function of their natural counterparts.[1,2] Peptoids are a class of robust, information-rich, chemically-diverse peptidomimetic polymers composed of *N*-substituted glycine monomers.[3] Like peptides, they have the ability to adopt distinct secondary structures such as ribbons,[4] helices,[5,6] sheets,[7] turns,[8] and cyclic structures;[9,10] however, the lack of a backbone hydrogen bond donor (NH) and chirality forces peptoid oligomers to conform to different folding rules as compared to their peptide counterparts.[11] Peptoids can be engineered to adopt multiple two and three-dimensional supramolecular assemblies including superhelices,[12] multi-helical bundles[13,14] and two-dimensional nanosheets.[15] These peptoid nanostructures self-assemble in an aqueous environment and are stabilized through networks of non-covalent interactions. Although peptoid polymers themselves are resistant to proteolysis and robust to chemical and physical stresses, their non-covalent higher order assemblies are susceptible to mechanical and chemical degradation.[16]

A broad family of peptoid polymers, all with an alternating pattern of ionic and hydrophobic monomers, self-assemble into unique, free-floating peptoid bilayers (Fig. 1a and b).[15] Peptoid nanosheets have been shown to act as robust scaffolds capable of displaying sequence-defined loops on their surface, mimicking the hierarchical structure of proteins.[17] These engineered nanosheets can perform specific functions such as the molecular recognition of proteins,[17] or templating the growth of inorganic materials.[18] These peptoid nanosheets, while robust under mild conditions, are susceptible to degradation when exposed to chemical or physical stress.[16] For example, upon exposure to harsh environments (*e.g.* pH < 5, $>30\%$ acetonitrile), or after a freeze/thaw cycle, nanosheets begin to break down and a significant reduction in size, particle counts and order (indicated by the presence of straight edges) is observed by fluorescence microscopy.[16]

In order for peptoid nanosheets to have broader utility, we sought to improve their stability by chemically crosslinking the chains to one another, after the sheets are assembled.

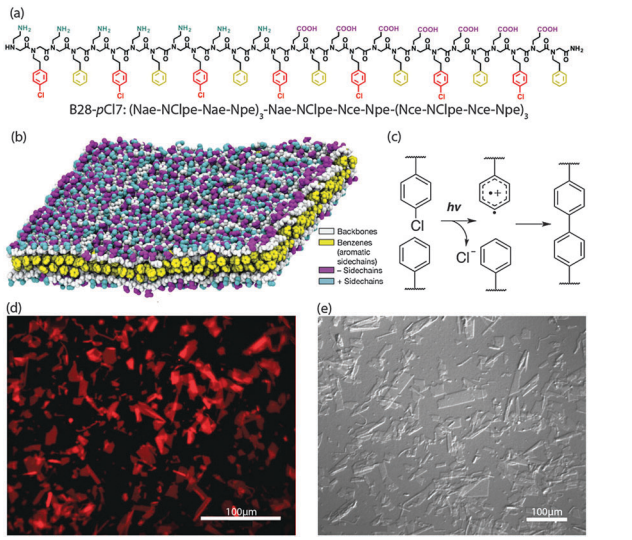

Fig. 1 (a) Chemical structure of photoactive sheet forming peptoid (B28-*p*Cl$_7$, M_W: 4119.63 g mol^{-1}). (b) Snapshot of unchlorinated peptoid nanosheet bilayer obtained from molecular dynamics simulation.[7] (c) Scheme for the photo-crosslinking reaction. Images of B28-*p*Cl$_7$ nanosheets obtained by (d) fluorescence microscopy and (e) by differential interference contrast microscopy.

The Molecular Foundry, Lawrence Berkeley National Laboratory, 1 Cyclotron Road, Berkeley, California 94720, USA. E-mail: rnzuckermann@lbl.gov

† Electronic supplementary information (ESI) available: Synthesis procedure for peptoid polymers; assembly conditions for nanosheet formation; photo-crosslinking procedure; SDS PAGE sample preparation procedure; AFM, XRD, and Raman spectroscopy sample preparation procedures; procedures for mechanical and chemical stability tests. See DOI: 10.1039/c6cc00588h

We further sought to introduce the crosslinks into the hydrophobic, aromatic-rich central core of the structure, so as not to interfere with solvent-exposed surface residues. Here we present a simple, photochemical method to selectively crosslink a portion of the aromatic groups to each other.

The canonical nanosheet-forming peptoid polymers utilize *N*-(2-phenylethyl)glycine monomers to form the hydrophobic core.[15] To minimize changes to the chemical structure of the sequence, we chose to install *N*-2-(4-chlorophenyl)ethyl glycine monomers at every other hydrophobic position (Fig. 1a). This subtle modification allows for the integration of a photoactive handle for the selective crosslinking of the nanosheet hydrophobic core, while minimally perturbing its ability to self-assemble into nanosheets (Fig. 1d and e).[19,20] In particular, the chloro substituted monomer was selected over the more labile Ar-halides (*e.g.* Ar–Br or Ar–I) due to its smaller size and lower hydrophobicity. The *para*-position was chosen to minimally perturb the aromatic packing of the hydrophobic core and has been previously shown to be well-tolerated.[17] The chlorinated amine submonomer, 2-(4-chlorophenyl)ethylamine, is also cheap and commercially available.

Although efficient transition-metal-free arylations are reported for aryl bromides and iodides, most require extreme conditions[21–23] – strong base (*e.g.* KO*t*Bu) and high temperatures (up to 200 °C) – not suitable for peptoid nanosheets. However, the mild photo-generated transition-metal-free arylation of 1-*t*-butyl-4-chlorobenzene to give 4-*t*-butyl-1,1′-biphenyl in ~70% yields in protic solvents was recently reported.[24] The photolytic cleavage of the aryl–chlorine bond results in formation of a triplet phenyl cation, which can subsequently undergo an electrophilic aromatic substitution with another phenyl ring (Fig. 1c). Although not as versatile as the transition metal mediated arylations, numerous biaryl species have been produced in this way.[25,26] In our case, we would expect the chlorophenyl groups to be in close proximity to several neighboring and apposing phenyl groups, and upon exposure of an aqueous nanosheet solution to ultraviolet radiation (254 nm), numerous biphenyl crosslinks should form.

The chlorinated nanosheet forming peptoid polymer (referred to as B28-*p*Cl$_7$, Fig. 1a) was synthesized by the previously reported automated solid phase submonomer method and purified by preparative reversed phase HPLC.[17,27] Nanosheets were then formed in aqueous solution (at 20 μm peptoid concentration) *via* the vial rocking method.[20,27] Nanosheet crosslinking was achieved by exposing a 4 mL glass open vial containing 500 μL (5 mm deep solution) of 20 μM peptoid nanosheet solution to 254 nm UV light for up to 3 hours (see ESI† for details).

The extent of nanosheet crosslinking reaction was monitored both by polyacrylamide gel electrophoresis (PAGE) analysis (typically used for proteins), to follow the increase in molecular weight of the peptoid chains, as well as by Raman spectroscopy to follow the conversion of functional groups, from chlorophenyl to biphenyl. A nanosheet solution was UV irradiated for various lengths of time, and the production of high molecular weight adducts and concurrent disappearance of peptoid monomers was examined by PAGE on a 4–20% gel (Fig. 2). Irradiated sheet solutions were concentrated and denatured in a buffered sodium dodecyl sulphate (SDS) solution prior to analysis. A single band, corresponding to the unreacted monomer in the non-irradiated sample, began to disappear, as higher molecular weight bands began to appear after 15 minutes of irradiation. After 2 hours only very high molecular weight adducts are observed that do not migrate down the gel, and by 3 hours there is almost no visible band observed to enter the gel. This is consistent with a significant increase in the degree of crosslinking within the nanosheet.

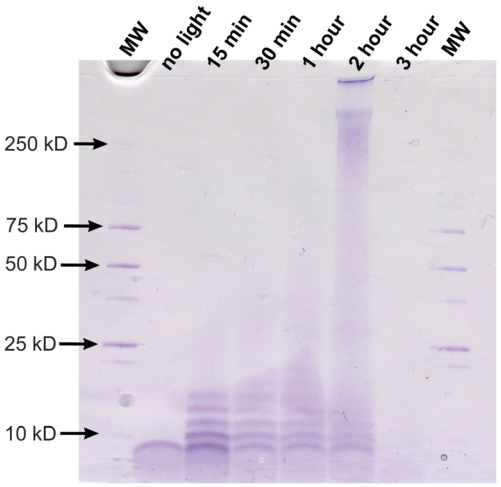

Fig. 2 SDS-PAGE (4–20%) analysis of denatured non-irradiated (lane 1) and crosslinked nanosheets, irradiated at 254 nm for different times (lanes 2–6).

In order to follow the conversion of the functional groups, Raman spectroscopy was performed during the course of the reaction. Analysis of nanosheets deposited onto a glass substrate through a drop and dry method revealed the appearance of a C–C bridge biphenyl stretching mode[28,29] at 1290 cm^{-1} and the disappearance of a chlorobenzene ring-breathing mode at 1090 cm^{-1} (Fig. 3).[30] There is also an obvious intensity increase C–C in plane phenyl stretching mode[31] at 1605 cm^{-1}. All of these observations are consistent with an internal crosslinking reaction occurring, generating biphenyl-like species at the expense of the chlorobenzene species.[18] Analysis of peak intensity changes after crosslinking suggest that the approximate reaction conversion is 45%.

Due to the loss of chlorine atoms and the formation of crosslinks, the nanosheet thickness is expected to change upon crosslinking. Nanosheet structure was probed using powder X-ray diffraction (XRD) and atomic force microscopy (AFM). Standard non-chlorinated peptoid nanosheets (B28) have a characteristic thickness of 2.7 nm (Fig. 4a).[15] By XRD it was observed that the *p*-chloro substitution increases the nanosheet thickness to 3.25 nm, which decreases to 2.97 nm upon irradiation (Fig. 4a), an observation consistent with the liberation of chlorine and formation of a biphenyl bridge in the nanosheet interior. These measurements were supported by AFM, which showed a thickness decrease from 3.31 ± 0.17 nm to 3.19 ± 0.24 nm upon crosslinking (Fig. 4b). Powder XRD analysis also revealed that the peptoid inter-strand spacing remained relatively unchanged at 4.65 Å, 4.65 Å, and 4.5 Å for

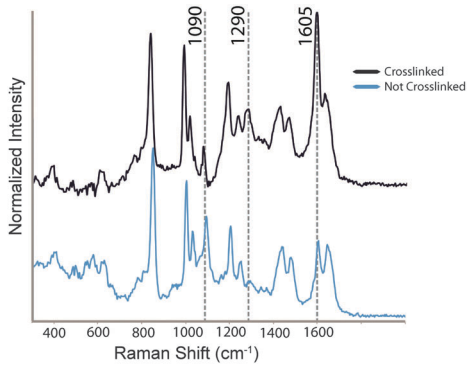

Fig. 3 Raman spectra of dried, crosslinked and non-crosslinked B28-pCl_7 nanosheets with Ph–Cl ring breathing mode, biphenyl C–C bridge stretching mode, and Ph ring stretching mode highlighted at 1090 cm^{-1}, 1290 cm^{-1}, and 1605 cm^{-1} respectively.

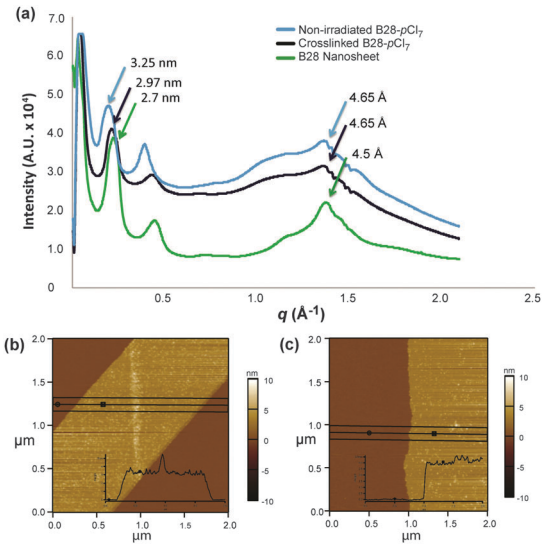

Fig. 4 (a) Powder XRD traces of pelleted non-chlorinated standard B28 nanosheets, non-irradiated B28-pCl_7 nanosheets, and B28-pCl_7 nanosheets irradiated at 254 nm for 3 hours. (b) AFM image of non-irradiated B28-pCl_7 nanosheet displaying a thickness of 3.31 ± 0.17 nm (c) AFM image of B28-pCl_7 nanosheets irradiated at 254 nm for 3 hours displaying thickness of 3.19 ± 0.24 nm.

the non-crosslinked, crosslinked, and unmodified sheets respectively (Fig. 4a). This indicates that the overall nanosheet structure is minimally perturbed by the monomer modification (*p*-Cl substitution) and the photo-crosslinking process. The fact that the inter-strand spacing is unchanged by crosslinking may also indicate that crosslinking occurs between the top and bottom leaflets of the nanosheets as opposed to between strands in the same leaflet.

To probe the resistance of crosslinked nanosheets to mechanical stress, sheet samples were first subjected to sonication for 30 minutes in a bath sonicator.[16] Aliquots of the sonicated samples were stained with Nile red and imaged by fluorescence microscopy. After thirty minutes of sonication, the average particle size of the non-crosslinked sheets decrease significantly, while numerous large ordered sheets, indicated by the presence of straight edges, exist in the crosslinked sample (Fig. 5a).

To further demonstrate stability of nanosheets to basic biochemical manipulations, solutions were lyophilized or centrifuged to a pellet, resuspended in buffer, and then analyzed by fluorescence microscopy. Samples to be lyophilized were first dialyzed against water, frozen at −80 °C and then lyophilized overnight. The resulting dry powder was resuspended in 10 mM tris buffer pH 8 by gently mixing with a pipet. The crosslinked nanosheets proved to be extremely robust to the lyophilisation procedure while the non-crosslinked sheets are almost completely destroyed (Fig. 5b). Samples to be pelleted were spun at 13.2k rpm in a microcentrifuge for 20 min. The supernatant was decanted and the pellet was resuspended, by pipet mixing, in fresh buffer and imaged *via* fluorescence microscopy. The crosslinked sheets again proved extremely robust to this procedure (Fig. 5c). While the non-crosslinked sheets are not completely destroyed, a marked size and population decrease was observed. This obvious increase in mechanical stability greatly increases the possible applications of peptoid nanosheets. The crosslinked nanosheets are now able to withstand standard biochemical manipulations, making them suitable platform on which to conduct a variety of assays.

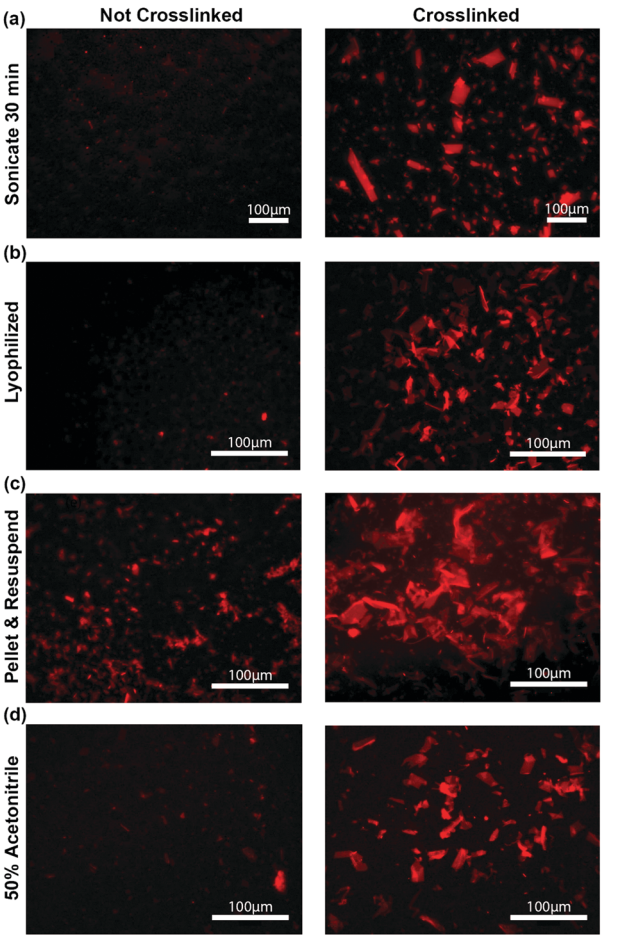

Fig. 5 Fluorescence microscopy images of nanosheets stained with Nile red. All rows show non-crosslinked nanosheets (left) and crosslinked nanosheets (right) after: (a) sonication for 30 min; (b) lyophilisation and resuspension; (c) pelleting and resuspension; (d) exposure to 50% acetonitrile for 20 min.

To assess the resistance of crosslinked sheets to organic solvent, crosslinked and non-crosslinked sheets were treated with 50% acetonitrile for 20 minutes at room temperature. Once again the crosslinked sheets remained intact under these harsh conditions, while the non-crosslinked sheets were dramatically reduced in size (Fig. 5d).

In an attempt to shorten irradiation times, the effect of oxygen inhibition on the crosslinking reaction was explored. A nanosheet solution in a glass vial was purged with nitrogen for 20 minutes and then sealed with a quartz coverslip and silicone grease, prior to irradiation. The production of high molecular weight adducts was monitored with irradiation time by PAGE analysis as above. These modified reaction conditions had a negligible effect on the rate of the reaction, leading to the conclusion that oxygen was not inhibiting the crosslinking reaction significantly.

In conclusion, we have developed a general approach to dramatically increase the chemical and mechanical stability of peptoid nanosheets. Rationally designed, sequence-defined peptoid oligomers with photolabile handles were synthesized using solid phase submonomer synthesis. Upon assembly into peptoid nanosheets, and subsequent exposure to UV light, a robust two-dimensional biomimetic nanomaterial is produced that proves extremely resistant to sonication, lyophilisation, pelleting, and environments of high organic solvent. Analysis by SDS PAGE, XRD, AFM, and Raman spectroscopy all confirm photocrosslinking within the nanosheet bilayer core. These highly robust crosslinked nanosheets are likely to find applications in a wide variety of biochemical assays, serve as better templates for synthesizing novel 2D nanomaterials, and better withstand harsh, non-aqueous environments.

This project was funded by the Defense Threat Reduction Agency under Contract No. DTRA10027-15875 and the DARPA Fold F(x) program. The work was conducted at the Molecular Foundry with support from the Advanced Light Source, at Lawrence Berkeley National Laboratory, both of which are supported by the Office of Science, Office of Basic Energy Sciences, U. S. Department of Energy under Contract No. DEAC02-05CH11231. We also thank R. Garcia, M. Connolly and B. Rad for their insightful discussions and inspiration. C. P. is grateful for a postdoctoral fellowship from the Natural Sciences and Engineering Council of Canada (NSERC).

Notes and references

1 A. S. Knight, E. Y. Zhou, M. B. Francis and R. N. Zuckermann, *Adv. Mater.*, 2015, **38**, 5665–5691.
2 J. Sun and R. N. Zuckermann, *ACS Nano*, 2013, **7**, 4715–4732.
3 N. Gangloff, J. Ulbricht, T. Lorson, H. Schlaad and R. Luxenhofer, *Chem. Rev.*, 2015, DOI: 10.1021/acs.chemrev.5b00201.
4 J. A. Crapster, I. A. Guzei and H. E. Blackwell, *Angew. Chem., Int. Ed.*, 2013, **52**, 5079–5084.
5 J. R. Stringer, J. A. Crapster, I. A. Guzei and H. E. Blackwell, *J. Org. Chem.*, 2010, **75**, 6068–6078.
6 C. W. Wu, T. J. Sanborn, K. Huang, R. N. Zuckermann and A. E. Barron, *J. Am. Chem. Soc.*, 2001, **123**, 6778–6784.
7 R. V. Mannige, T. K. Haxton, C. Proulx, E. J. Robertson, A. Battigelli, G. L. Butterfoss, R. N. Zuckermann and S. Whitelam, *Nature*, 2015, **526**, 415–420.
8 O. Roy, C. Caumes, Y. Esvan, C. Didierjean, S. Faure and C. Taillefumier, *Org. Lett.*, 2013, **15**, 2246–2249.
9 S. B. Y. Shin, B. Yoo, L. J. Todaro and K. Kirshenbaum, *J. Am. Chem. Soc.*, 2007, **129**, 3218–3225.
10 C. Tedesco, L. Erra, I. Izzo and F. De Riccardis, *CrystEngComm*, 2014, **16**, 3667–3687.
11 G. L. Butterfoss, P. D. Renfrew, B. Kuhlman, K. Kirshenbaum and R. Bonneau, *J. Am. Chem. Soc.*, 2009, **131**, 16798–16807.
12 H. K. Murnen, A. M. Rosales, J. N. Jaworski, R. A. Segalman and R. N. Zuckermann, *J. Am. Chem. Soc.*, 2010, **132**, 16112–16119.
13 B.-C. Lee, T. K. Chu, K. A. Dill and R. N. Zuckermann, *J. Am. Chem. Soc.*, 2008, **130**, 8847–8855.
14 B.-C. Lee, R. N. Zuckermann and K. A. Dill, *J. Am. Chem. Soc.*, 2005, **127**, 10999–11009.
15 E. J. Robertson, A. Battigelli, C. Proulx, R. V. Mannige, T. K. Haxton, L. Yun, S. Whitelam and R. N. Zuckermann, *Acc. Chem. Res.*, 2016, DOI: 10.1021/acs.accounts.5b00439.
16 R. Kudirka, H. Tran, B. Sanii, K. T. Nam, P. H. Choi, N. Venkateswaran, R. Chen, S. Whitelam and R. N. Zuckermann, *Pept. Sci.*, 2011, **96**, 586–595.
17 G. K. Olivier, A. Cho, B. Sanii, M. D. Connolly, H. Tran and R. N. Zuckermann, *ACS Nano*, 2013, **7**, 9276–9286.
18 J. M. V. Jun, V. Altoe, S. Aloni and R. N. Zuckermann, *Chem. Commun.*, 2015, **51**, 10218–10221.
19 B. Sanii, T. K. Haxton, G. K. Olivier, A. Cho, B. Barton, C. Proulx, S. Whitelam and R. N. Zuckermann, *ACS Nano*, 2014, **8**, 11674–11684.
20 B. Sanii, R. Kudirka, A. Cho, N. Venkateswaran, G. K. Oliver, A. M. Olson, H. Tran, R. M. Harada, L. Tan and R. N. Zuckermann, *J. Am. Chem. Soc.*, 2011, **133**, 20808–20815.
21 H. Liu, B. Yin, Z. Gao, Y. Li and H. Jiang, *Chem. Commun.*, 2012, **48**, 2033–2035.
22 Y. S. Ng, C. S. Chan and K. S. Chan, *Tetrahedron Lett.*, 2012, **53**, 3911–3914.
23 Y. Qiu, Y. Liu, K. Yang, W. Hong, Z. Li, Z. Wang, Z. Yao and S. Jiang, *Org. Lett.*, 2011, **13**, 3556–3559.
24 H. Qrareya, C. Raviola, S. Protti, M. Fagnoni and A. Albini, *J. Org. Chem.*, 2013, **78**, 6016–6024.
25 M. Fagnoni and A. Albini, *Acc. Chem. Res.*, 2005, **38**, 713–721.
26 S. Lazzaroni, S. Protti, M. Fagnoni and A. Albini, *Org. Lett.*, 2009, **11**, 349–352.
27 H. Tran, S. L. Gael, M. D. Connolly and R. N. Zuckermann, *J. Visualized Exp.*, 2011, **57**, e3373.
28 D. Lin-Vien, N. B. Colthup, W. G. Fateley and J. G. Grasselli, *The Handbook of Infrared and Raman Characteristic Frequencies of Organic Molecules*, Academic Press, San Diego, CA, 1991.
29 C. Zhu, G. Meng, Q. Huang, Z. Zhang, Q. Xu, G. Liu, Z. Huang and Z. Chu, *Chem. Commun.*, 2011, **47**, 2709–2711.
30 J. H. S. Green, *Spectrochim. Acta, Part A*, 1970, **26**, 1503–1513.
31 S. Stewart and P. M. Fredericks, *Spectrochim. Acta, Part A*, 1999, **55**, 1641–1660.

